Journal of Catalysis **211,** 19–32 (2002)
doi:10.1006/jcat.2002.3714

A New Monte Carlo Model for Supported-Catalyst Sintering

Allen G. Sault*,[1,2] and Veena Tikare†

*Catalytic and Porous Materials Department MS 1349 and †Materials & Process Modeling Department MS 1411, Sandia National Laboratories, Albuquerque, New Mexico 87185

Received June 7, 2001; revised June 5, 2002; accepted June 10, 2002

We present a new 2D Monte Carlo model of supported-catalyst sintering that is capable of generating all known catalyst sintering behaviors, including atom emission and recapture (Ostwald ripening), particle migration and coalescence, and vapor-phase transport. This model differs from previously reported phenomenological models in that no mechanism is presupposed; rather sintering is allowed to arise naturally from atomic-scale interactions among metal atoms and the support. The model uses a classical Metropolis algorithm to determine movement of metal atoms on a support. The metal–support system is represented by a two-dimensional rectangular mesh oriented perpendicular to the support surface. The top and bottom rows of the mesh represent the support, so that the total mesh represents a long, narrow pore. The simulations are initialized by placing metal atoms into the mesh to obtain a desired initial state. The Metropolis algorithm randomly selects a metal atom and a neighboring site and, if the neighboring site is empty, moves the metal atom to the neighboring site with a probability proportional to $\exp(-\Delta E/kT)$, where ΔE is the change in energy associated with the move. Energies of the initial and final states are calculated from pairwise interactions between the sites involved and their nearest neighbors. The simulation is run for 10^6–10^7 Monte Carlo time steps (MCS), where a single MCS corresponds to a number of attempted moves equal to the number of metal atoms in the simulation. Our model bears certain resemblances to previously published Monte Carlo models but introduces several improvements. First, our model properly calculates probabilities of metal atom migration by using the change in energy associated with the move, rather than simply using the energy of the initial state. Second, our model includes sites in the center of the pore and can therefore model gas-phase transport of metal atoms. Earlier models used a two-dimensional mesh oriented parallel to the support surface and, therefore, did not include sites corresponding to the gas phase. Third, our choice of two-dimensional plane allows modeling of contact angles between metal particles and the support. Countering this advantage is our inability to model the shape of the contact surface between the metal particles and the support. Finally, because our two-dimensional model includes gas-phase sites, generalization to three dimensions is conceptually simple, requiring only the extension of the mesh in the third dimension. Extension of the earlier models to three dimensions would require inclusion of new concepts since the gas phase is not present in the two-dimensional plane chosen. © 2002 Elsevier Science (USA)

Key Words: **sintering; catalyst sintering; Monte Carlo; supported catalyst.**

INTRODUCTION

Sintering of supported metal particles is gaining renewed attention as a result of increasingly stringent automotive emissions requirements, and the consequent need for more efficient usage of precious metals such as Pt, Pd, and Rh, commonly used in catalytic converters. Metal particles grow rapidly during the initial stage of catalytic converter use and continue to grow, albeit at a slower rate, throughout catalyst lifetimes. For this reason, catalytic converters initially contain far more precious metals than are needed. The excess metal content allows the catalyst to continue to meet regulatory requirements as particle sizes increase during use. Similar issues exist within the refining industry, where supported catalysts play key roles in many processes. The extreme temperatures (1073 K) that can occur in catalytic converters make this problem particularly acute for the automotive industry.

If methods could be developed to mitigate sintering in supported catalysts, emission requirements could be met for the required catalyst lifetimes while using far smaller amounts of precious metals. Unfortunately, the primary mechanisms contributing to catalyst sintering remain controversial, and until this controversy is resolved development of strategies to control sintering will be difficult. Three potential mechanisms for sintering have been proposed: (i) particle migration and coalescence, (ii) atom emission and recapture (also known as Ostwald ripening), and (iii) vapor-phase transport. In the first mechanism, particle migration and coalescence, metal particles migrate by a random walk on the support surface. When two particles collide, they coalesce to become one particle. The second mechanism, atom emission and recapture, involves surface diffusion of metal atoms on the support surface. The chemical potential of smaller particles is higher than that of larger particles, as formalized by the Gibbs–Thomson equation.

[1] To whom correspondence should be addressed. Fax: (505)845-0541. E-mail: agsault@sandia.gov.

[2] Current Address: MS 0807, Sandia National Laboratories, Albuquerque, NM 87185-0807.

0021-9517/02 $35.00
© 2002 Elsevier Science (USA)
All rights reserved.

Atoms preferentially diffuse from the smaller, high-potential metal particles to the larger, low-potential ones. Thus, large particles grow at the expense of small ones. The third mechanism, vapor-phase transport, arises from the same driving force for particle growth as in the previous mechanism. However, the atom transport mechanism is evaporation of atoms from the smaller particles and precipitation onto larger ones. These mechanisms were the subject of several reviews in the 1970s (1–7), which also describe attempts to model and predict the behavior arising from the various mechanisms. The predictions were compared to experiments to determine the sintering mechanism in supported-catalyst particles. Unfortunately, the quality of experimental data is often not sufficient to allow reliable conclusions to be drawn, as exemplified by one particular debate in the literature (8, 9).

The models proposed in the 1970s are largely phenomenological, assuming a certain mechanism and then deriving particle size distributions expected from that mechanism. The underlying atomic-scale physical phenomena are often not directly incorporated into the models. More recently, Bartholomew (10–12) has shown that virtually all available catalyst sintering data can be fit to a second-order generalized power law expression (GPLE) proposed by Fuentes and Ruiz-Trevino (13). While this model allows quantitative comparisons to be made among different catalysts, it does not provide any discrimination among sintering mechanisms since both particle migration and coalescence and Ostwald ripening are second-order processes.

In 1988 Campbell *et al.* (14) simulated catalyst sintering using a two-dimensional Monte Carlo (MC) model that does not make any *a priori* assumptions regarding sintering mechanisms, but rather simulates sintering as a result of atomic-scale processes involving pairwise interactions between atoms. More recently, Lo and Skodje (15, 16) proposed a similar model for investigating two-dimensional island diffusion and evaporation on surfaces. As discussed below, there are areas in which we feel that these models are inaccurate, but they nevertheless show that MC techniques based on atomic-scale interactions can result in both particle migration and coalescence and Ostwald ripening. Although this result does not prove that the two mechanisms arise from the same underlying physical effect, it does show that the possibility must be considered. The third mechanism, vapor-phase transport, could not be modeled by Campbell *et al.* or Lo and Skodje since they both modeled the catalyst as a flat support plane with rafts of metal atoms representing the particles, and no gas-phase was present.

In this paper, we present a MC model to simulate supported-catalyst sintering that bears certain similarities to the models of Campbell *et al.* and Lo and Skodje, but which corrects certain problems in their approaches. In addition to verifying that both particle migration and coalescence and Ostwald ripening can arise from a random motion of individual atoms, our model also simulates particle faceting, wetting of the support by metal particles, and vapor-phase transport. In this initial report, we do not attempt to model a specific metal–support system or to attain agreement with experiment but content ourselves with demonstrating that the model simulates all of the known catalyst sintering behaviors and can provide information about metal particle growth resulting from these behaviors. Thus, simulation parameters will be chosen that facilitate observation of the desired behaviors in reasonable computational times without regard to whether the parameters are physically realistic or represent actual metal–support systems. We briefly discuss initial simulations using physically realistic parameters, and in the conclusion discuss refinements necessary to allow this algorithm to simulate more-realistic systems.

ALGORITHM

The kinetic Monte Carlo model used in this study to simulate catalyst sintering is adapted from a similar model used to simulate Ostwald ripening in bulk materials whereby particles at a liquid–solid interface dissolve, diffuse through the liquid, and precipitate on the surface of another grain (17). In order to simulate supported-catalyst sintering, the model was adapted to simulate particle migration and Ostwald ripening with transport of metal atoms by surface diffusion and vapor-phase transport. For simplicity we have chosen not to include grain growth in the simulations reported here, although this is easily incorporated into the algorithm (18).

Microstructure Representation

A two-dimensional square lattice normal to the support surfaces was used to represent the catalyst–support system, as shown in Fig. 1. The lattice is populated by integers that

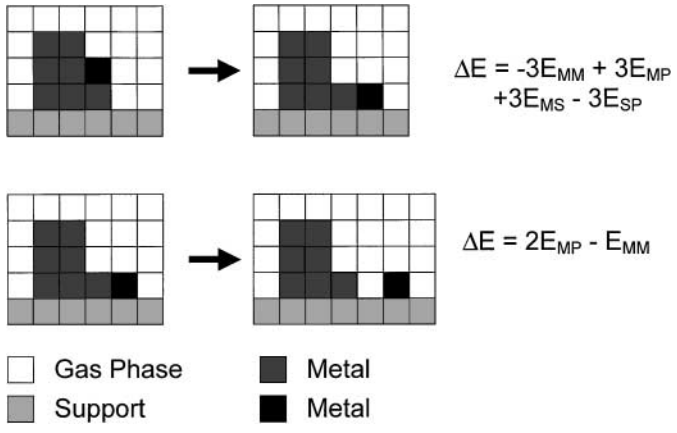

FIG. 1. Schematic diagram showing the rectangular lattice used to simulate catalyst microstructure. Calculations of ΔE for two prototypical sintering events are shown.

identify the lattice sites as the support (−2), occupied by a metal atom (1), or gas phase (−1). The simulation space is typically rectangular, with a large-aspect ratio to represent a long, narrow pore with periodic boundary conditions at each end of the pore. The system is initialized by placing semicircular metal particles at random locations along the walls of the pore. The particle size, particle size distribution, and number of particles are input by the user and particles are not allowed to overlap initially. The support sites are fixed and are not allowed to move during the simulation. Our simulations differ from the MC simulations of Campbell *et al.* (14) and Lo and Skodje (15, 16) in that the two-dimensional plane chosen here is perpendicular to the support surface, while the previous studies used a plane parallel to the support. One advantage of the choice made here is that the gas phase is represented and it is possible to observe gas-phase transport of metal atoms. A second advantage is that the simulations can model wetting and spreading of metal particles on the support and contact angels between the metal and support can be observed. Third, because our 2D model contains gas-phase sites, extension to three dimensions is conceptually simple, requiring only extension of the simulation mesh into the third dimension and proper accounting for interactions between sites in the third direction. The models of Campbell *et al.* and Lo and Skodje do not include the gas phase, so extension to three dimensions would not be nearly as straightforward. Offsetting the advantages described above is the fact that our model cannot simulate particle shapes and faceting in the plane parallel to the surface. In addition, the one-dimensional nature of the surface in our model restricts both atom and particle motion. An atom emitted by one particle can only return to the emitting particle or migrate to the neighboring particle; it cannot move around a neighboring particle to be incorporated into any other particle on the surface. Similarly a given particle can only coalesce with one of the two neighboring particles. As long as the surface coverage is realistic, this limitation should not influence the rate of particle–particle coalescence or the rate at which emitted atoms are recaptured. The 1-D nature of the surface does severely limit the number of potential coalescence partners for a given particle and may thereby artificially limit the range of allowed results. This limitation is accepted in our model in order to obtain the important advantages noted above and to provide information that complements previous modeling efforts. Furthermore, by including a sufficiently large number of particles in the simulation it is possible to overcome this limitation statistically. By systematically increasing the size of the simulation until the results cease to change, it would be possible to determine the number of particles required to ensure statistically significant results. For this initial study we have chosen to concentrate on the qualitative capabilities of the model, leaving such statistical studies for future work.

Energies of State

Sintering in catalysts is driven by interfacial energies. The energy of the system is defined as the sum of all neighboring pairwise interaction energies for all sites in the simulation,

$$E_{\text{total}} = \frac{1}{2}\sum_{i=1}^{N}\sum_{j=1}^{M} E_{ij}, \qquad [1]$$

where E_{ij} is the interaction energy of the atom at site i with its neighbor at site j, N is the total number of sites in the simulation, and M is the number of neighbors being considered. In our simulations we assume that the four nearest-neighbor interactions are equivalent to the four next-nearest-neighbor interactions, so that $M = 8$.

The interaction energies in our model result from a summing of pairwise interaction energies between neighboring sites. Four pairwise energies are used: metal–metal (E_{MM}), metal–support (E_{MS}), metal–pore (E_{MP}), and support–pore (E_{SP}). The first two energies have a clear physical meaning provided each occupied site in the lattice is assumed to represent a single atom. In this case E_{MM} is the metal–metal pairwise bond energy, which can be calculated from tabulated heats of sublimation (19), and E_{MS} is the metal–support pairwise bond energy. Recent advances in measurement of heats of adsorption of metals on oxides (20) are beginning to provide accurate experimental values for E_{MS}, as are *ab initio* calculations of metal bonding on oxide surfaces (21, 22). E_{MP} and E_{SP} do not have a direct physical meaning but can be related to measurable physical quantities, namely, surface free energies. Employing a thought experiment involving splitting bulk metal and support materials to form surfaces, it can be shown that the relationships

$$\gamma_{\text{MP}} = \left(\frac{\varepsilon_{\text{MM}}}{2} - \varepsilon_{\text{MP}}\right), \qquad [2]$$

$$\gamma_{\text{SP}} = \left(\frac{\varepsilon_{\text{SS}}}{2} - \varepsilon_{\text{SP}}\right), \qquad [3]$$

$$\gamma_{\text{SM}} = \left(\frac{\varepsilon_{\text{MM}}}{2} + \frac{\varepsilon_{\text{SS}}}{2} - \varepsilon_{\text{MS}}\right), \qquad [4]$$

hold, where γ_{MS}, γ_{MP}, and γ_{SP} are the surface energies (energy/unit length in 2D) at the three interfaces in the system, and ε is the bonding energy per unit surface length between the various phases. ε is simply related to E by $\varepsilon_{\text{AB}} = 3E_{\text{AB}}(N/A_v)$, where N is the number of atoms per unit surface length, and A_v is Avogadro's number. The factor of three arises from the need to break three bonds between each atom and three of its neighbors to form the surface. Thus, by varying pairwise interactions energies, the interfacial energies can be varied during the simulations. Clearly γ_{MP} and γ_{SP} are influenced by the composition of the gas phase, making it meaningful to include E_{MP} and E_{SP}

in the simulations and discuss the effects of changes in these parameters on sintering behavior.

With these equations and independent knowledge of E_{MM} and E_{MS} (see above), values of E_{MP}, E_{SS}, and E_{SP} can be determined if the surface tensions (which are roughly approximated by surface energies) are known. While surface tensions of liquid metals are known (23), surface tensions of solid metals, support oxides, and metal-oxide interfaces are not, although Ruckenstein (7) estimated values for interfacial free energies of metals and oxides at relevant temperatures by assuming a linear relationship between temperature and energy. For the simulations presented here, we choose E_{MS} and E_{SP} to facilitate observation of sintering rather than attempting to obtain accurate values. Note that E_{MS} and E_{SP} can have signs opposite to E_{MM} and E_{MS}, since surfaces are generally energetically unfavorable.

Microstructural Evolution Simulation Algorithm

The algorithm works by selecting a metal site at random and selecting one of the eight neighboring sites also at random. If the neighboring site is unoccupied, an exchange of the two sites is attempted. If the neighboring site is another metal site or a support site, no exchange is possible and a new metal site/neighbor pair is chosen. This is repeated until a metal site with an unoccupied neighbor site is found. An exchange of these two sites is then attempted. Two typical site exchanges are shown in Fig. 1. The energy change (ΔE) accompanying the exchange is calculated using Eq. [1] and a classical Metropolis algorithm (24) is used to determined whether the exchange will be accepted. More details of the Metropolis algorithm and example calculations corresponding the prototypical sintering events in Fig. 1 are given in the Appendix.

Simulation Parameters

Each simulation is performed for a fixed number of Monte Carlo steps (MCS), where one MCS corresponds to the number of attempted exchanges equal to the total number of occupied sites in the simulation. Although these calculations do not provide a true time, it can be shown that the MCS time scale is proportional to real time (25, 26). Typically at least 10^6–10^7 MCS are required to observe significant sintering with the parameters we have chosen. Images of the sintering process are taken and particle size statistics calculated at times corresponding to 1, 2, . . . , 9, 10, 20, . . . , 80, 90, 100, 200, 300, . . . , MCS. Typical simulations reported here require approximately 3 days of CPU time running on a DEC Alpha 8400 Enterprise server with 4 Gbytes of RAM and a 440-MHz CPU.

Earlier, we assumed that each occupied site represents a single atom in order to assign a clear physical meaning to E_{MM} and E_{MS}. The assumption of atomic-size cells is also necessary to place the simulations in the proper physical size range. Sintering is most severe for particles with sizes ranging from 1 to 10 nm; larger particles tend to sinter much more slowly or not at all, except under extreme conditions. For typical metal atom diameters of 0.22–0.25 nm, a simulated 1.0-nm particle corresponds to a diameter of four to five sites, while a 10-nm particle corresponds to 40–45 sites. If instead we assume that a single site represents multiple atoms, then such small particles would be represented by an unrealistically small number of cells and the simulated behavior would not model the real behavior. Note that in bulk sintering studies (17, 18) in which particles can have a wide range of length scales, such an assumption is not made and each cell is an indeterminate size.

The assumption of atomic-size cells is also consistent with the assumption of a single-grain orientation (no grain growth). For atom emission and recapture it clearly makes no sense to talk of grain orientations for single atoms, as an atom that collides with a particle will automatically assume the orientation of the particle. For particle migration and coalescence grain orientation could be important, but some treatments suggest that grain growth is rapid relative to migration and can therefore be neglected (1).

The decision to model events on an atomistic level severely limits the time scale of the simulations, given the applied computational power. If one takes a typical value of 10^{13} s^{-1} for the preexponential factor for atom movements, then each atom attempts to move once every 0.1 ps, corresponding to a single MCS. With 10^7 MCS, the total time of the simulations is therefore only on the order of 1 μs, far below the time scale over which supported-catalyst sintering typically occurs. A similar problem exists in the previous Monte Carlo studies (14–16). We will discuss in the conclusion possible code optimizations and computational resources that will help to overcome this limitation. At this point, it is important to reiterate that the goal of this work is to demonstrate the ability of the model to generate known sintering behaviors, not to quantitatively model specific experimental data. The latter goal will only be realized as the code is further optimized and more-powerful computing resources are employed.

RESULTS

Particle Migration

An enduring controversy in the sintering literature involves the relative importance of particle migration vs atom emission and recapture (Ostwald ripening). It has been noted that particle migration most likely occurs by surface diffusion of atoms over the particle surface, with random fluctuations causing atoms to accumulate on one side of the particle. The net result of these fluctuations is Brownian motion of the particle on the support (1). In order to investigate whether our model simulates particle migration, we performed simulations beginning with a single particle in a 30×300 cell lattice and monitored the position of the

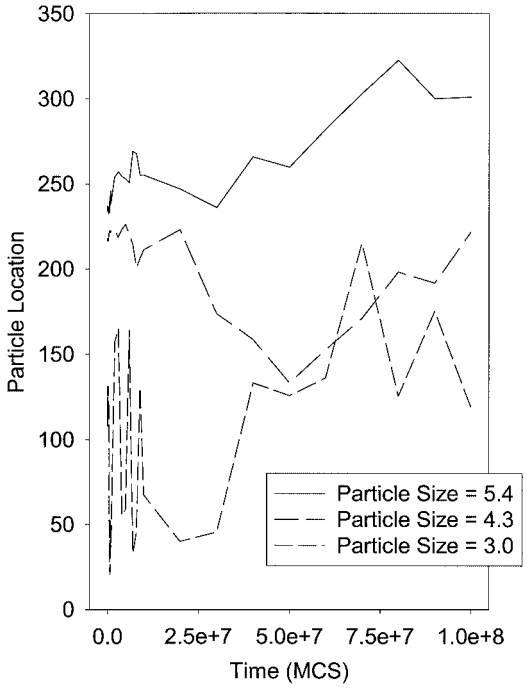

FIG. 2. Motion of single particles in a pore as a function of particle size. The centers of mass of the particles are plotted as a function of time. $E_{MM}/kT = -2.86$, $E_{MS}/kT = -1.43$, and $E_{SP}/kT = E_{MP}/kT = 0.71$.

particle center of mass along the length of the pore as a function of time. Assuming an atom diameter of 0.25 nm, this lattice corresponds to a pore diameter of 7.5 nm and a length of 75 nm. Of course, the periodic boundary conditions result in an effectively infinite pore length. Results are shown in Fig. 2 for particles with sizes ranging from 3 to 5.4. Particle size is simply defined as the square root of the number of occupied cells in the particle. Values of the various interaction energies are given in the figure caption.

The results clearly show that on average smaller particles move a greater distance than larger particles over a given time interval. Based on the result in Fig. 2 it is tempting to calculate average migration distances and compare the results to theoretical formulations, such as those proposed by Wynblatt and Gjostein (1), who showed that average migration distance, X_p, is related to particle size through the relationship

$$X_p = 2\sqrt{(D_p t)}, \qquad [5]$$

where $D_p = 0.301 D_s\,(a/R)^4$ is the particle diffusivity, D_s is the surface diffusion coefficient of the metal, R is the particle size, and a is the atomic diameter. However, closer inspection of the simulation results shows that such a comparison is not valid. Within our model, the site exchange algorithm gives rise not only to particle migration but also to atom emission, and there is no way to guarantee that particles stay intact during the simulation. In small particles, atom emission can completely dissociate the particles, or even result in transport of atoms from one side of the pore to the other, a process that can only occur as a result of vapor-phase transport. Such behavior was observed during the simulations shown in Fig. 2. These results make it meaningless to analyze particle motion in the context of Eq. [5]. A similar conclusion was noted by Lo and Skodje for small particle sizes (15, 16).

Sintering Simulations—High Particle Density

Sintering simulations involving multiple particles were performed in a 30×3000 cell pore, approximating a pore with a 7.5-nm diameter and 750-nm length. The number of metal atoms was kept constant at a value of 6300, while the initial particle sizes, the temperature, and the values of the various interaction energies were varied. Results for an initial particle size of 7.94 and a typical set of conditions are shown in Fig. 3. After only a few MC time steps, the particles retain their semicircular shape and no sintering is apparent. After 8000 time steps, several changes are apparent. First, several pairs of particles that were initially close together have begun to coalesce, resulting in dumbbell-shaped particles sometimes observed in experimental sintering studies (27). The coalescence appears to result from wetting and spreading of neighboring particles, rather than from particle migration, consistent with the limited mobility of particles of size greater than 6, which can be inferred from Fig. 2. While the wetting effect is to some extent a result of the semicircular initial shape of the particles, statistical fluctuations in particle shapes would result in coalescence of closely spaced particles even if an equilibrium shape is chosen for the initial state. Second, particle shapes have changed from semicircular to faceted. Surfaces either parallel to, perpendicular to, or at a 45° angle to the support plane are prevalent. Faceting is more apparent at lower temperatures. Faceting was not observed by Campbell *et al.* (14) in their MC study, probably because temperatures were too high. The faceting is clearly a result of surface free energy minimization, as the observed faceting planes display the highest possible coordination numbers for surface atoms. Third, atom emission is apparent after 8000 MCS though difficult to see in Fig. 3b, manifesting itself by the appearance of individual atoms bound to the support surface. Finally, vaporization of metal atoms is also apparent at the bottom right of Fig. 3b. Thus, based on this single simulation, we conclude that our model is capable of simulating all known supported-catalyst sintering behaviors.

After 85,000 MCS further changes are apparent. Particle coalescence continued until the dumbbell-shaped particles noted after 8000 MCS assumed more rounded shapes with some evidence of faceting, and additional pairs of neighboring particles coalesced. Certain particles migrated short distances, and other particles grew at the expense of neighboring particles, providing clear evidence for both particle

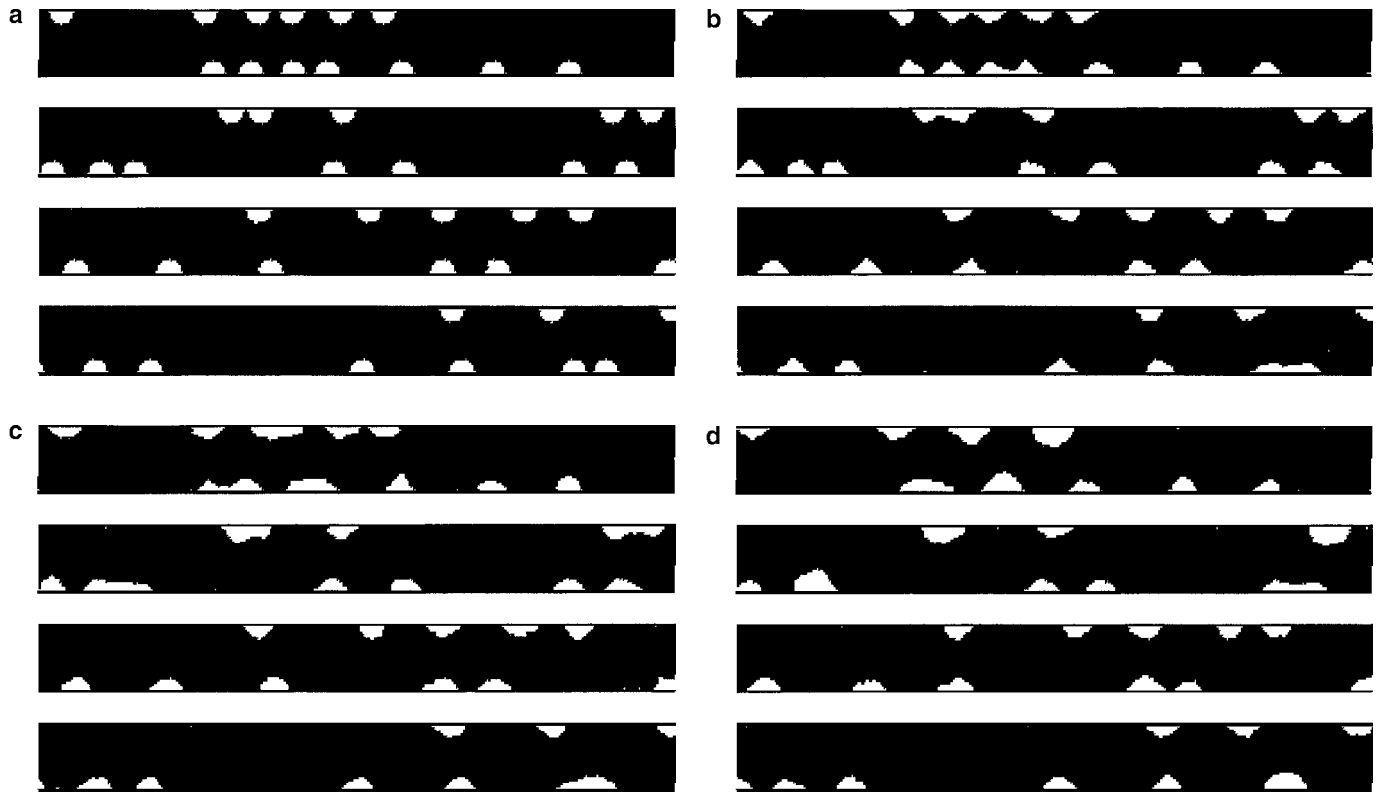

FIG. 3. Simulated evolution of metal particles in a 30×3000 cell pore initially containing 100 metal particles of size 7.94: (a) 8, (b) 8,000, (c) 90,000, and (d) 900,000 MCS. Only four 30×300 cell sections of the pore are shown. $E_{MM}/kT = -2.0$, $E_{MS}/kT = -1.0$, and $E_{SP}/kT = E_{MP}/kT = 0.5$.

migration and Ostwald ripening. Results after 850,000 MCS continue these trends. Clearly, all known supported-catalyst sintering mechanisms are operative under the conditions of this simulation.

Particle growth is plotted in Fig. 4 for different initial particle sizes and particle size distributions. The average particle size in Fig. 4 is calculated as the arithmetic mean of all particles containing three or more atoms. Single atoms and dimers are not considered to be particles. First consider curve a, which corresponds to the simulation in Fig. 3. Particles grow rapidly during the first 5000 MCS as a result of rapid coalescence of closely spaced pairs of neighboring particles, noted earlier. Subsequent increases in average particle size are much slower as the growth mechanism shifts from coalescence of closely spaced particles to particle migration and coalescence and/or Ostwald ripening. Clear evidence for Ostwald ripening is provided by the particle size distributions shown in Fig. 5. After 90,000 MCS the particle size distribution is bimodal, showing two discrete regions, corresponding to particles that have coalesced and essentially doubled in size and to particles that have not coalesced. As time progresses, the bimodal distribution broadens and a wide range of particle sizes are noted. This broadening can only occur as a result of atom emission and recapture. Since atom emission and recapture

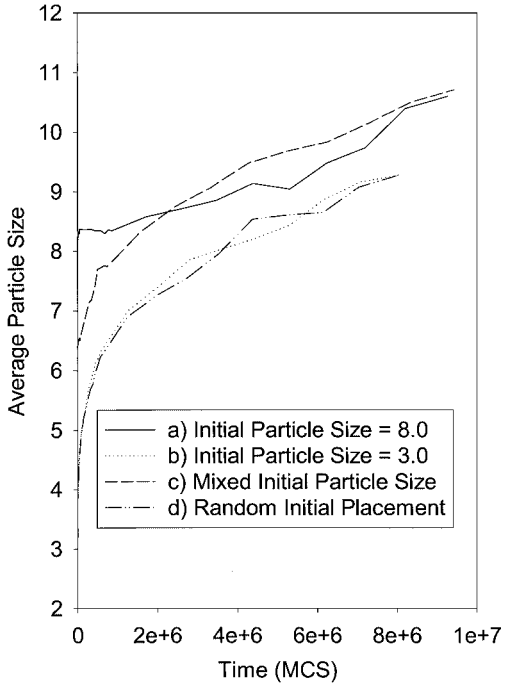

FIG. 4. Particle growth curves as a function of initial particle size for a 30×3000 cell pore. All simulations involve 6300 metal atoms, but the initial number of metal particles varies due to the different initial particle sizes. $E_{MM}/kT = -2.0$, $E_{MS}/kT = -1.0$, and $E_{SP}/kT = E_{MP}/kT = 0.5$.

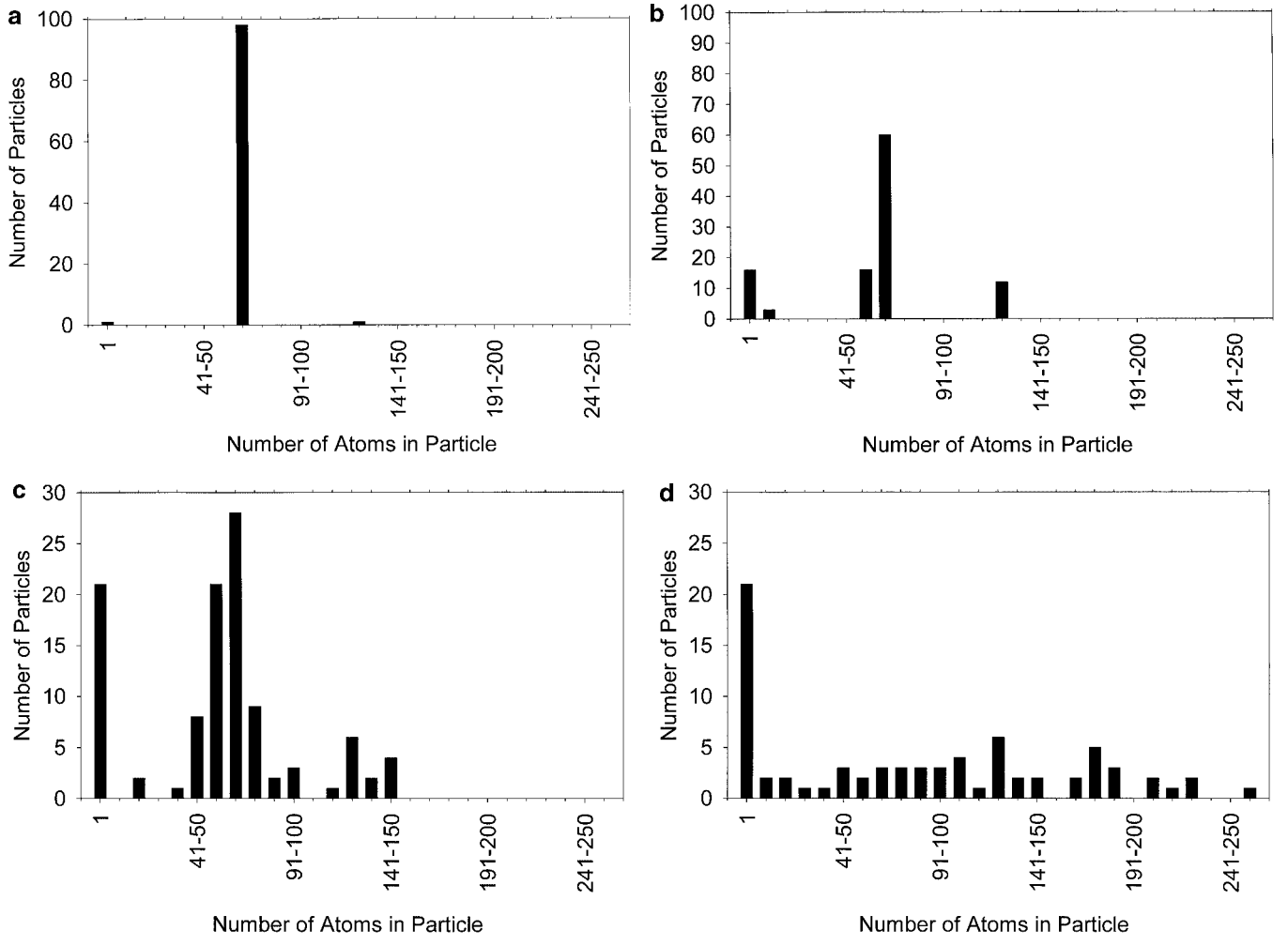

FIG. 5. Particle size distributions for the simulation shown in Fig. 4a with an initial particle size of 7.94: (a) 8, (b) 90,000, (c) 900,000, and (d) 9×10^6 MCS.

is not separable from particle migration and coalescence in our model, it is not readily apparent whether the continuing increase in average particle size at long times results primarily from particle migration and coalescence or from Ostwald ripening. It is clear, however, that the initial rapid particle size growth is due to wetting and spreading of closely spaced particles, leading to coalescence, while the slower growth at long times requires either particle migration and coalescence or Ostwald ripening, or a combination of both.

Particle growth for an initial particle size of 3.0 is plotted in curve b of Fig. 4. Because the number of metal atoms in the simulation is kept constant, there are initially seven times as many particles present initially in this simulation as in the simulation of size 7.94 particles (Fig. 4, curve a). For this reason, smaller, more mobile, and more closely spaced particles give rise to much faster particle growth by coalescence at early times than is observed in Fig. 4, curve a. As the simulation progresses, the rate of particle growth slows in a smooth but noticeable manner. This rate decrease can be attributed to one of two factors. It may signal a shift from an initial rapid particle coalescence mechanism caused by wetting and spreading to slower particle growth resulting from particle migration and coalescence and/or Ostwald ripening. The absence of a sharp break between these two regimes, as observed for size 8.0 particles (Fig. 4, curve a), would then be attributed to an extended period of particle coalescence via wetting and spreading resulting from the higher initial number density of particles. Alternatively, the rate decrease could simply arise from a slowing of the rates of both particle migration and atom emission as particle size increases. Initial rapid particle coalescence can clearly be seen in the histograms in Fig. 6, which show that after only a few MCS some particles are four times larger than their initial particle size and it must therefore result from multiple coalescence events. Atom emission followed by surface diffusion and vapor transport is evident during the entire simulation, since single atoms are seen and the particle sizes become distributed (Fig. 6).

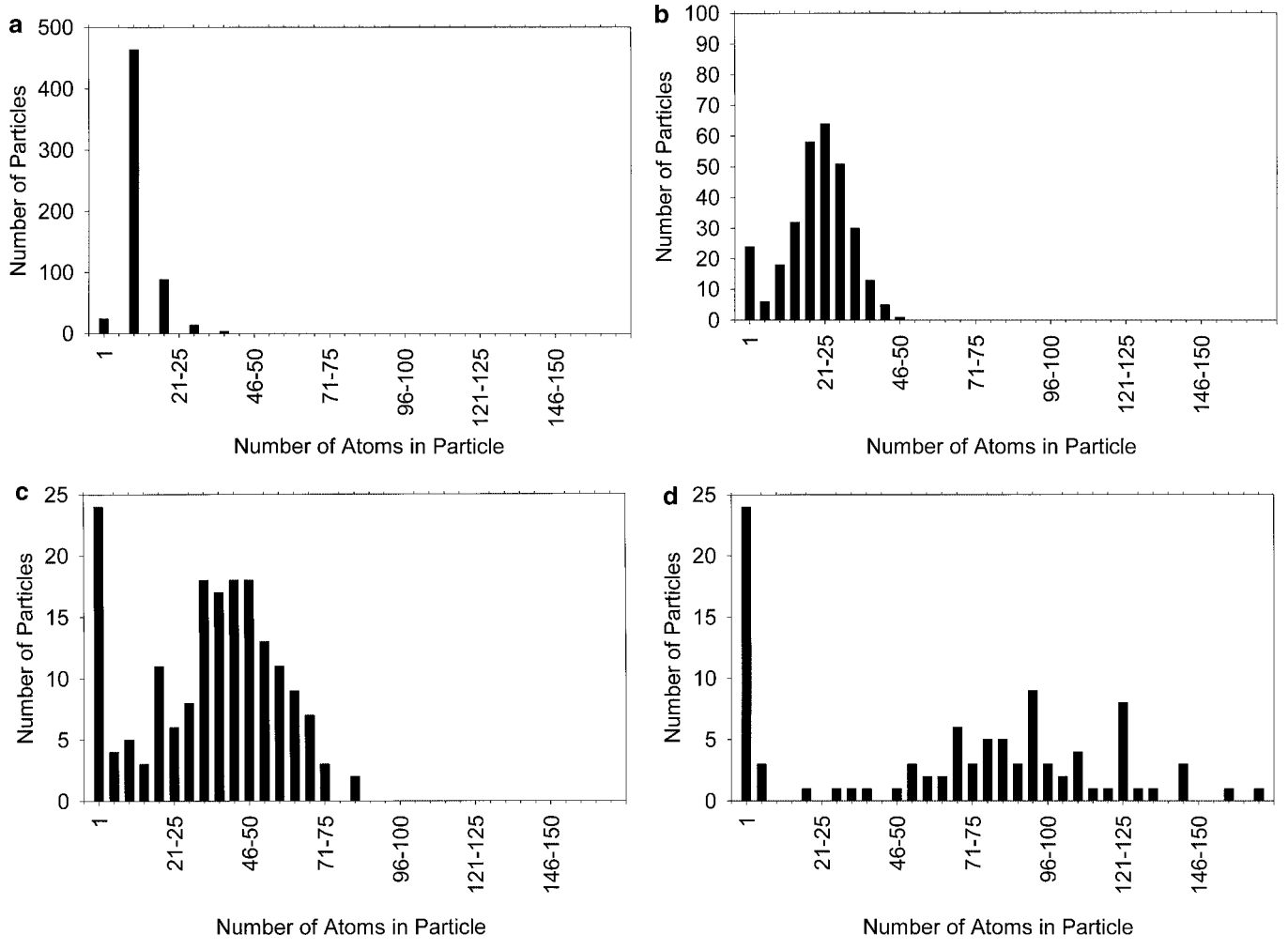

FIG. 6. Particle size distributions for the simulation shown in Fig. 4b with an initial particle size of 3.0: (a) 4, (b) 50,000, (c) 600,000, and (d) 8×10^6 MCS.

Two other curves in Fig. 4 show sintering starting with a mixed initial size distribution (Fig. 4, curve c), and random placement of individual atoms along the pore walls (Fig. 4, curve d). In the former case, the initial average particle size is ~6.1, but the initial particle coalescence stage increases the average particle size rapidly and the results become equivalent to those for an initial particle size of 7.94 after ~2,000,000 MCS. For the random starting configuration, results are indistinguishable from an initial particle size of 3.0. This occurs because the extremely high number of size 3.0 particles (700) and their small size result in an initial configuration that is not very different from that resulting from random placement of individual atoms.

Particle growth at different simulation temperatures is plotted in Fig. 7 and particle growth for different interaction energies is plotted in Figs. 8–11. Most of the effects are as expected, but there are some interesting subtleties that bear discussion. In Fig. 8, sintering rates increase as E_{MM} decreases in magnitude, due to the decreased energy required to emit an atom from a particle. For the lowest absolute value of E_{MM}, however, the average particle size actually *decreases* during the initial stages of the simulation. The explanation for this phenomenon was first advanced by Campbell *et al.* (14). Isolated atoms on the support can be thought of as a one-dimensional lattice gas in equilibrium with the metal particles. As $|E_{MM}|$ decreases, the equilibrium pressure of this lattice gas increases and more atoms must be emitted to achieve equilibrium, resulting in a decrease in the average particle size. Establishment of this equilibrium is much faster than the initial rate of particle growth, with the result that average particle size undergoes an initial decrease prior to particle growth. In a typical supported-catalyst preparation involving metal loading by incipient wetness followed by calcining and hydrogen reduction, it is to be expected that an equilibrium concentration of isolated atoms would be achieved during preparation, so this effect is not likely to be observed experimentally.

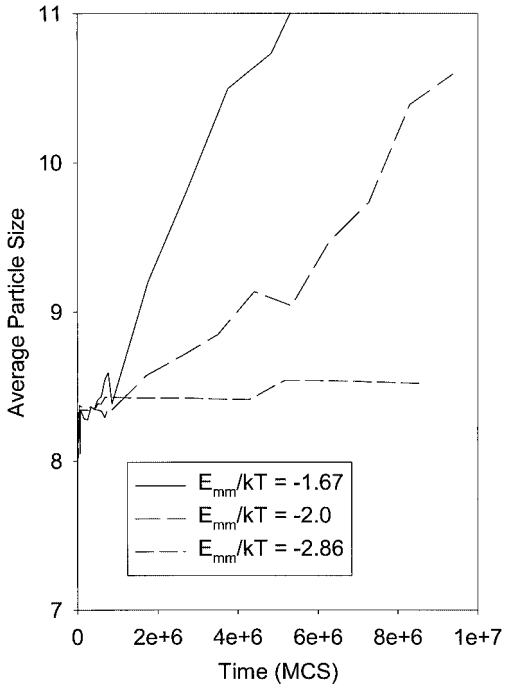

FIG. 7. Temperature dependence of sintering in a 30×3000 cell pore initially containing 100 metal particles of size 7.94. $E_{MM}/E_{MS} = 2.0$, $E_{MM}/E_{SP} = -4.0$, and $E_{MP} = E_{SP}$.

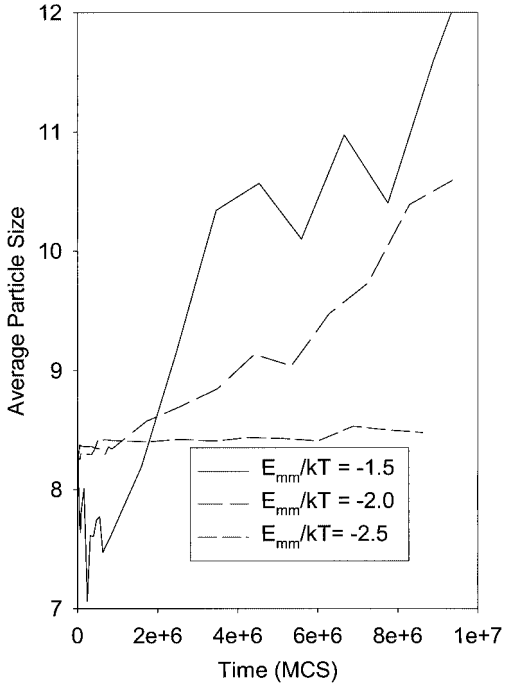

FIG. 8. Dependence of sintering on E_{MM}/kT in a 30×3000 cell pore initially containing 100 metal particles of size 7.94. $E_{MS}/kT = -1.0$ and $E_{SP}/kT = E_{MP}/kT = 0.5$.

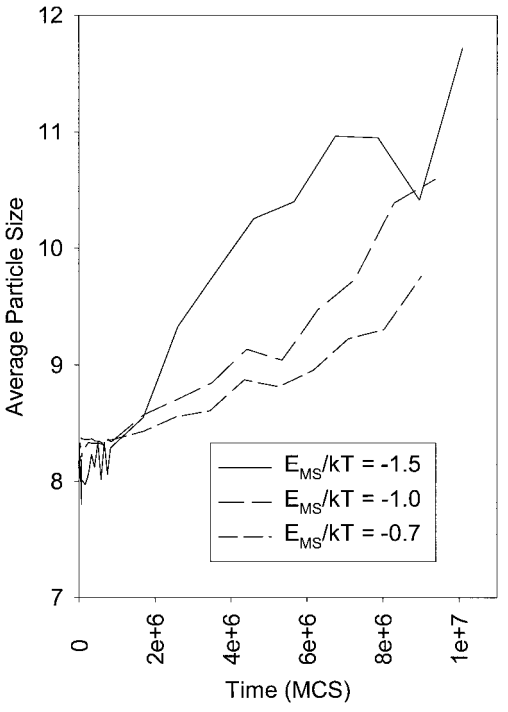

FIG. 9. Dependence of sintering on E_{MS}/kT in a 30×3000 cell pore initially containing 100 metal particles of size 7.94. $E_{MM}/kT = -2.0$ and $E_{SP}/kT = E_{MP}/kT = 0.5$.

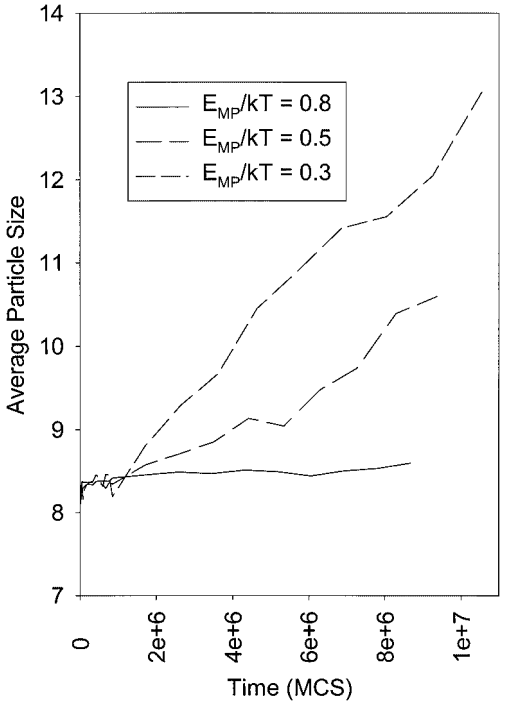

FIG. 10. Dependence of sintering on E_{MP}/kT in a 30×3000 cell pore initially containing 100 metal particles of size 7.94. $E_{MM}/kT = -2.0$, $E_{MS}/kT = -1.0$, and $E_{SP}/kT = 0.5$.

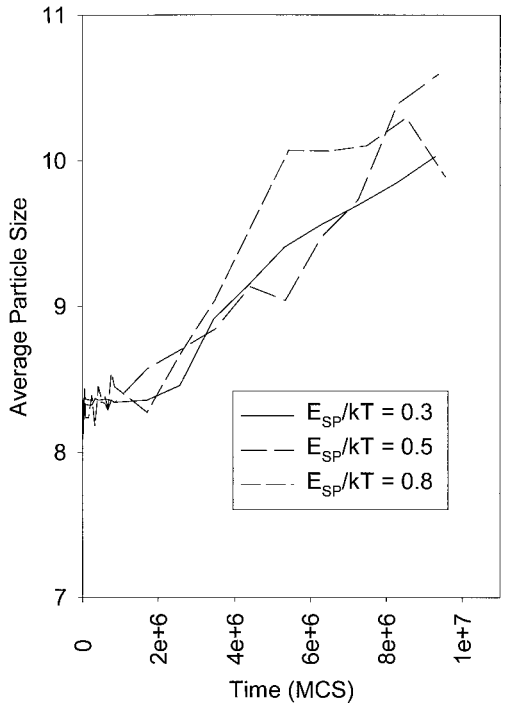

FIG. 11. Dependence of sintering on E_{SP}/kT in a 30×3000 cell pore initially containing 100 metal particles of size 7.94. $E_{MM}/kT = -2.0$, $E_{MS}/kT = -1.0$, and $E_{MP}/kT = 0.5$.

Another unexpected result is observed in Fig. 11, which shows that E_{SP} has no discernable effect on sintering rates. An explanation for this result can be found in the schematic diagram of prototypical sintering events that occur in these simulations (Fig. 1). While the calculation of ΔE for one of the processes shows a dependence on E_{SP}, E_{SP} is much smaller in magnitude than E_{MM} or E_{MS} so the overall effect is weak and E_{SP} has a negligible effect on sintering rates. Similar analyses of the two expressions for ΔE provide explanations for the observed decrease in sintering rate with increasing $|E_{MM}|$, the increase in sintering rate with increasing $|E_{MS}|$, and the increase in sintering rate with decreasing $|E_{MP}|$.

Sintering Simulations—Low Particle Density

The particle densities used for the simulations in Figs. 3–11 are extremely high, corresponding to a metal coverage of more than a monolayer (ML) (6300 metal atoms on 6000 support sites). Few real catalysts have metal loadings high enough to result in such coverages. A catalyst with 1.0 wt% Pt supported on 300 m^2/g alumina corresponds to only 0.01 ML of Pt. It would require 30 wt% Pt on a support with a surface area of 100 m^2/g to achieve a full monolayer. Nevertheless, the high-coverage simulations are useful, as they enhance the rates of sintering and allow the operative phenomena to be observed in a relatively short time.

Having demonstrated the various sintering phenomena with the high-coverage simulations, we next performed simulations at more realistic coverages using a total of 6300 metal atoms, but with a $30 \times 30{,}000$ cell pore. In this case, metal coverage corresponds to only 0.1 ML. Results for the $30 \times 30{,}000$ cell pore are compared to the 30×3000 cell pore in Fig. 12. Sintering rates are substantially lower for the lower metal loading regardless of initial particle size. In fact, for size 8 particles at low coverage, the average particle size decreases throughout the simulation. This decrease arises from the need to establish equilibrium between the particles and the one-dimensional lattice gas of isolated atoms, as discussed earlier. With a factor of 10 decrease in particle density, 10 times more atoms must be emitted from each particle to establish this equilibrium. The simulations confirm this analysis, with 20–25 isolated atoms present on average in the high-particle-density simulation, but more than 250 in the low-particle-density simulation. Evidently, the sintering processes cannot overcome this initial loss of metal atoms over the time scale of the simulation. Note also that there is no initial rapid jump in average particle size for the low-coverage simulations, due to the lower likelihood that two particles will be close enough at the start of the simulation to spread and coalesce rapidly. For the smaller particle sizes substantial sintering is seen at both particle densities, but the rate is much lower for the low-particle-density simulations, in keeping with the greater

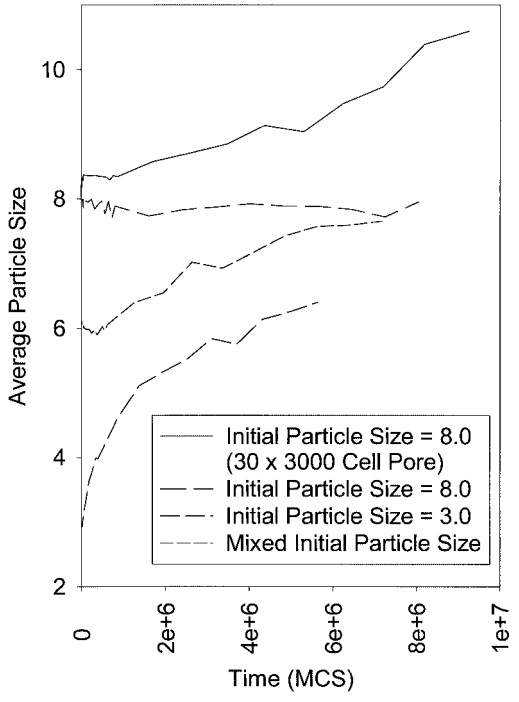

FIG. 12. Particle growth curves as a function of initial particle size for a $30 \times 30{,}000$ cell pore. $E_{MM}/kT = -2.0$, $E_{MS}/kT = -1.0$, and $E_{SP}/kT = E_{MP}/kT = 0.5$.

average distance between particles and the resulting slower rate of transfer of atoms between particles.

Generalized Power Law Analysis

Fuentes and Ruiz-Trevino (13) proposed a generalized power law expression (GPLE) to describe sintering rates, which has been extensively evaluated by Bartholomew (10–12) and shown to be widely applicable. The expression takes the form

$$-d(D/D_0)/dt = k(D/D_0 - D/D_{eq})^m, \qquad [6]$$

where D is the catalyst dispersion (percentage of metal atoms located at the gas–metal interface; D is inversely proportional to particle diameter), D_0 is the initial dispersion, m is an integer equal to 1, 2, or 3, and k and D_{eq} are fitting parameters that correspond to a sintering rate constant and a pseudoequilibrium dispersion obtained at long sintering times, respectively. Bartholomew has shown that a second-order expression with $m = 2$ best fits most data. With $m = 2$, integration of the GPLE gives

$$D/D_0 = (kt + 1/(1 - D_{eq}/D_0))^{-1} + D_{eq}/D_0. \qquad [7]$$

In order to determine whether our simulations are consistent with the GPLE, selected data have been fit to the GPLE. Figure 13 shows that the fit for the $30 \times 30{,}000$ cell pore with initial particle size of 3.0 is excellent, but that fits for the 30×3000 cell data are relatively poor. These poor fits may be the result of a change in sintering behavior over the time scale of the simulation. As discussed earlier, during the initial stages of the simulation particle wetting/spreading and coalescence are operative, but at later stages either Ostwald ripening or particle migration and coalescence increases in importance. Since it is unlikely that the fitting parameters would be the same for two different behaviors, it is not surprising that fitting the entire data set gives poor results. If the range of data fitted is restricted to simulation times greater than 100,000 MCS, a region where the initial wetting/spreading and coalescence mechanism is no longer operative, the quality of the fit improves greatly. The high quality of the fit for the $30 \times 30{,}000$ cell simulation results from the fact that particle coalescence is not a significant contributor to sintering even at small times, so the entire data set can be fit with a single set of parameters.

Some of the data, such as that for size 7.94 particles in a 30×3000 cell lattice (Fig. 4, curve a), display almost no curvature over the time frame of the simulation. As a result, the data can be closely fit by Eq. [7], but physically unrealistic values of the parameters result, including negative values for D_{eq}. Extending the simulations for longer times would presumably result in noticeable curvature and physically realistic fitting parameters, but the computer time required for these extended simulations is currently prohibitive.

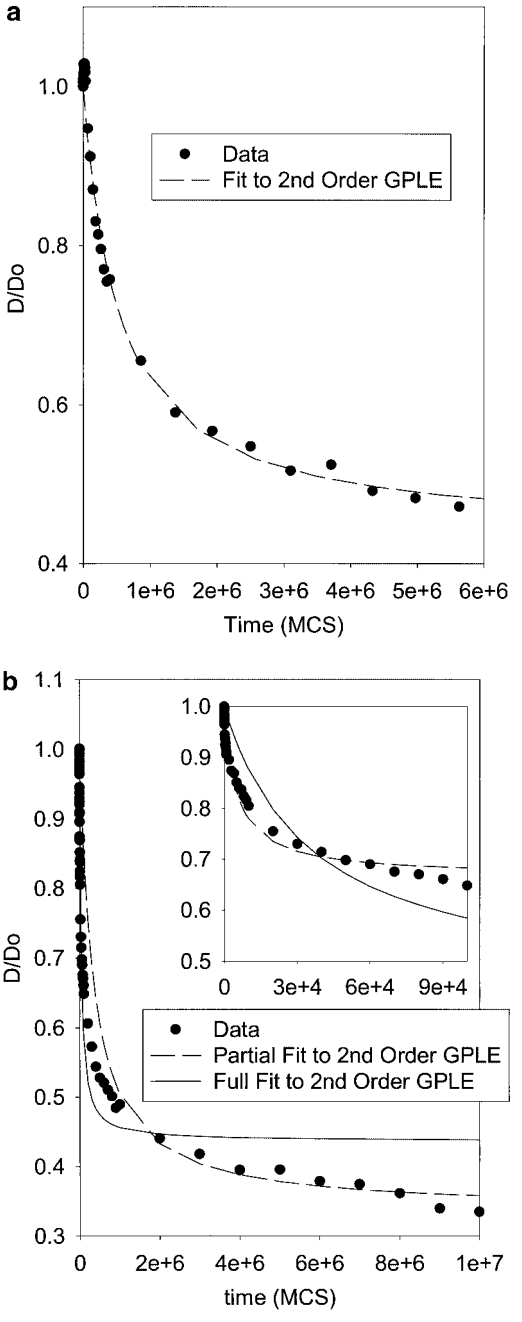

FIG. 13. Fit of sintering simulations to generalized power law expression. (a) $30 \times 30{,}000$ cell pore with initial particle size of 3.0. (b) 30×3000 cell pore with initial particle size of 3.0. $E_{MM}/kT = -2.0$, $E_{MS}/kT = -1.0$, and $E_{SP}/kT = E_{MP}/kT = 0.5$.

Log Normal Analysis

Nearly 25 years ago Granqvist and Buhrman (4–6) presented a conceptually simple model of supported-catalyst sintering that assumes particle coalescence as the only operative mechanism and predicts a log-normal distribution of particle sizes. They further claimed that available experimental data closely conformed to this model and concluded

that particle migration and coalescence is the most important mechanism for sintering. Wanke (8) disagreed with this analysis, however, claiming that Ostwald ripening models fit the data equally well, but his arguments were rebutted by Granqvist and Buhrman (9). Recently, Datye and coworkers (28) reexamined this issue and concluded that the log-normal size distribution is in fact frequently observed in experimental studies of sintering. The data obtained in our simulations show clear evidence for Ostwald ripening, and our particle size distributions therefore do not show the shape characteristic of a log-normal plot.

Note, however, that our simulations were designed to show the utility of our algorithm, not to model a particular metal–support system and obtain agreement with experiment. The parameters used were therefore chosen to demonstrate that all known sintering mechanisms can be simulated and to obtain significant sintering in a reasonable time and are not physically realistic. In particular, values of E_{MM}/E_{MS} range from 2 to 3 in our simulations, while the actual ratio for the Pt/Al_2O_3 system is closer to 10 (1). Also, absolute values of E_{MM}/RT are unrealistically low. For Pt, with a heat of sublimation of 564.4 kJ/mol (19) and 12 nearest neighbors, $E_{MM} = -564.4/6 = -94$ kJ/mol. A value of E_{MM}/RT of -2.0 therefore corresponds to a temperature over 5000 K! More realistic temperatures of ~1000 K, as frequently found in automotive catalytic converters, would result in $E_{MM}/RT \cong -11$. Even for metals with lower heats of sublimation, such as Pd or Cu, $E_{MM}/RT \cong -6$ for reasonable temperatures. Unfortunately, using these more realistic parameters results in negligible sintering, even after 5×10^6 MCS. Since 10^7 MC steps require 3 days of CPU time with a 440-MHz processor, extending the simulation time by orders of magnitude to observe sintering under these conditions is not feasible until program efficiency is dramatically improved, or a massively parallel implementation is made. As a result of these problems, we cannot currently determine whether a log-normal distribution can be simulated by our model, or equivalently whether simulation parameters can be chosen that allow particle migration and coalescence without allowing significant Ostwald ripening.

Particle Shape and Contact Angles

Young's equation relates the contact angle between a particle and a solid surface to the three surface tensions, which we approximate with surface energies (see Eqs. [2]–[4]):

$$\cos\theta = (\gamma_{SP} - \gamma_{MS})/\gamma_{MP}. \quad [8]$$

Substituting Eqs. [2]–[4] into 10 gives an approximate expression for $\cos\theta$ in terms of E:

$$\cos\theta = (E_{MS} - E_{SP} - E_{MM}/2)/(E_{MM}/2 - E_{MP}). \quad [9]$$

For the simulation presented in Fig. 3, Eq. [9] predicts $\theta = 71^\circ$. Since Young's equation is based on a continuum approximation and our simulations are discrete, a direct comparison with the simulations is not possible. Furthermore, random fluctuations result in a distribution of contact angles in the simulations. Nevertheless it is clear from Fig. 3 that contact angles are all between 45 and 90°, in agreement with the prediction. For the more realistic simulation discussed above, with $E_{MM}/RT = -6$ and $E_{MM}/E_{MS} = 10$, $\cos\theta$ is predicted to be ~130°. The simulations show a vast majority of contact angles near 135°, with a few near 90°. Similar analysis for all of the simulations attempted shows that the observed contact angles are in excellent qualitative agreement with the prediction.

CONCLUSIONS

A new two-dimensional kinetic Monte Carlo model for supported-catalyst sintering has been presented that is capable of simulating all known catalyst sintering behaviors. Particle migration/spreading and coalescence was simulated with increasing migration rates as particle size decreased. Ostwald ripening by surface diffusion and vapor-phase transport by atom emission and recapture were also simulated. All of these behaviors arise from a single underlying physical mechanism, namely, migration of metal atoms from occupied to unoccupied sites in the catalyst/support system. Although it may be possible to manipulate the parameters such that one behavior or another is dominant during the simulations, the different behaviors cannot be rigorously isolated and must all be considered as potential contributors to metal particle growth in supported catalysts.

The model provides information on particle shapes in the plane normal to the support and on contact angles between the support and the metal particles. The predicted shapes and contact angles are in good agreement with expected values. In cases where simulation data covers a sufficiently large time range and no change occurs in the dominant behavior over the time range of the simulation, data can be fit to the generalized power law expression of Fuentes and Ruiz-Trevino (13), in agreement with experimental data. The simulation results do not agree well with the log-normal distribution predicted by Granqvist and Buhrmann (4–6) for particle migration and coalescence, due to the fact that the simulation parameters chosen give rise to Ostwald ripening as a major sintering behavior. With different simulation parameters, it is likely that particle migration and coalescence could become dominant, resulting in better fits to the log-normal distribution.

Utilization of the model to simulate more-realistic systems and make more direct, quantitative comparisons with experiment is currently limited by computational power, code inefficiencies, and limitations introduced by

assumptions made during algorithm development. We are optimistic that optimization of the code combined with a massively parallel implementation and continued improvements in available hardware will allow three-dimensional simulations with realistic physical parameters without incurring unacceptably long execution times. For example, in bulk grain growth models methods have been developed to decrease execution time by *a priori* elimination of low- or zero-probability events (29). Application of such methods to catalyst sintering could eliminate consideration of moves in which the chosen atom has no empty nearest-neighbor sites and therefore has zero probability of moving. Execution times could also be substantially decreased by choosing metal atoms for attempted moves systematically rather than randomly. A systematic approach has been shown to be equivalent to the random approach for Potts-model grain growth simulations (30). Equivalence is also expected for the catalyst sintering problem and will yield substantial improvements in execution time by eliminating costly random number generation. Finally, implementation of the code for parallel computers offers the potential for decreasing execution time by three or more orders of magnitude. The catalyst sintering problem is well suited for parallel implementation, offering an obvious domain decomposition with minimal communication requirements.

In addition to decreasing program execution times, future work will also address assumptions made in development of the algorithm, including more-realistic calculations of pairwise bond energies, extension to hexagonal or cubic close-packed lattices, and inclusion of activation energies for metal atom movements. Although limiting the quantitative accuracy of the results, the assumptions made in the development of the algorithm greatly simplify the calculations while still allowing the generation of all known supported-catalyst sintering behavior and are therefore justified for these initial simulations.

Finally, we plan to apply the model to applications for which the currently available code and computing resources are more suitable. Current efforts in this area include 3D simulations of single-particle diffusion, particle evaporation rates, and equilibrium particle shapes (31). Because our two-dimensional model includes gas phase, support, and metal sites, extension to three dimensions required only extension of the lattice into the third dimension and proper accounting for nearest-neighbor interactions in all three directions. Studies of the effects of grain boundaries and defects in the support on sintering behavior are also candidates for future studies.

APPENDIX: METROPOLIS ALGORITHM AND SAMPLE CALCULATIONS

The Metropolis algorithm uses a change in energy (ΔE) to calculate the probability of a given event occurring. In our case ΔE is the difference in total energy between the initial and final states involved in the movement of a single metal atom to an adjacent unoccupied site. From Eq. [1] it is apparent that this ΔE can be calculated by considering only the interaction energies between the two sites involved in the movement and the neighboring sites. Considering the movement shown in the top half of Fig. 1, the metal atom to be moved initially has four metal atoms and four empty sites as neighbors. The interaction energy between this atom and its neighbors is therefore

$$E_{\mathrm{MI}} = 4E_{\mathrm{MM}} + 4E_{\mathrm{MP}}. \qquad [A1]$$

Similarly, the initially empty site has two metal atoms, three support atoms, and three empty sites as neighbors. Since we assume no interaction between empty sites, the interaction energy between the initial empty site and it neighbors is therefore

$$E_{\mathrm{EI}} = 2E_{\mathrm{MP}} + 3E_{\mathrm{SP}}. \qquad [A2]$$

A similar analysis of the final state shows that the final empty site has five metal atoms and three empty sites as neighbors, for an interaction energy of

$$E_{\mathrm{EF}} = 5E_{\mathrm{MP}}, \qquad [A3]$$

while the final position of the metal atom has one metal atom, three support atoms, and four empty sites as neighbors, for an interaction energy of

$$E_{\mathrm{MF}} = E_{\mathrm{MM}} + 3E_{\mathrm{MS}} + 4E_{\mathrm{MP}}. \qquad [A4]$$

The total change in energy for the prototypical move shown at the top of Fig. 1 is therefore

$$\begin{aligned}\Delta E &= E_{\mathrm{MF}} + E_{\mathrm{EF}} - E_{\mathrm{MI}} - E_{\mathrm{EI}} \\ &= -3E_{\mathrm{MM}} + 3E_{\mathrm{MP}} + 3E_{\mathrm{MS}} - 3E_{\mathrm{SP}}. \end{aligned} \qquad [A5]$$

A similar analysis of the metal atom movement shown at the bottom of Fig. 1 gives the value of ΔE shown in the figure.

If ΔE is negative, the reaction is exothermic and the exchange is accepted with a probability of 1.0. If ΔE is positive, the exchange is accepted with a probability of

$$P = \exp\left(-\frac{\Delta E}{kT}\right). \qquad [A6]$$

For a specific instance, a random number between zero and one is calculated and compared to P. If the random number is less than P, the move is accepted and the metal atom is moved to the formerly empty site. If the random number is greater than P, the move is rejected and the configuration of atoms is unchanged.

The model as presented here neglects activation barriers (E_a) for all atom movements and considers only the net

change in energy for every transition. This is equivalent to assuming that the activation energy is a constant for all processes, as this would simply change the probability of all transitions by a constant given by

$$P_{\text{activation}} = \exp\left(\frac{-E_a}{k_B T}\right). \quad [A7]$$

Of course, the greater the value of E_a, the smaller the probability of accepting a move, causing the rate of sintering to decrease. While this changes the time scaling of the simulations it does not alter the microstructural evolution of the system. By effectively choosing $E_a = 0$ in our simulations, the rate of sintering is accelerated, facilitating observation of microstructural changes.

In contrast to our method, both Campbell *et al.* (14) and Lo and Skodje (15, 16) only considered the initial energy of the system when calculating transition probabilities. As a result, the probability for accepting a move becomes

$$P = \exp\left(\frac{E_{\text{MI}} + E_{\text{EI}}}{kT}\right). \quad [A8]$$

With this equation, it is possible for an exothermic exchange to be less probable than an endothermic exchange, provided the initial state for the exothermic movement has a higher binding energy than the initial state for the endothermic movement. Since this situation is physically unrealistic, we feel that the use of ΔE in the Metropolis algorithm is more correct than use of the initial energy alone.

ACKNOWLEDGMENTS

The authors acknowledge Jason Mudd for assistance with generation of the histograms in Figs. 5 and 6, and for calculations of dispersion used in Fig. 13. The authors also acknowledge Abhaya K. Datye for informative discussions regarding comparisons between experiment and simulations. This work is supported by the U.S. Department of Energy under Contract DE-AC04-94AL85000. Sandia is a multiprogram laboratory operated by Sandia Corporation, a Lockheed Martin Company, for the United States Department of Energy.

REFERENCES

1. Wynblatt, P., and Gjostein, N. A., *Prog. Solid State Chem.* **9**, 21 (1975).
2. Wynblatt, P., Dalla Betta, R. A., and Gjostein, N. A., *in* "The Physical Basis for Heterogeneous Catalysis" (E. Drauglis, Ed.), p. 501. Plenum, New York, 1975.
3. Wanke, S. E., and Flynn, P. C., *Cat. Rev–Sci. Eng.* **12**, 93 (1975).
4. Granqvist, C. G., and Buhrman, R. A., *Appl. Phys. Lett.* **27**, 693 (1975).
5. Granqvist, C. G., and Buhrman, R. A., *J. Appl. Phys.* **47**, 2200 (1976).
6. Granqvist, C. G., and Buhrman, R. A., *J. Catal.* **42**, 477 (1976).
7. Ruckenstein, E., *in* "Metal Support Interactions in Catalysis, Sintering, and Redispersion" (S. A. Stevenson, J. A. Dumesic, R. T. K. Baker, and E. Ruckenstein, Eds.), p. 141. Van Nostrand Reinhold, New York, 1987.
8. Wanke, S. E., *J. Catal.* **46**, 234 (1977).
9. Granqvist, C. G., and Buhrman, R. A., *J. Catal.* **46**, 238 (1977).
10. Bartholomew, C. H., *Appl. Catal. A* **107**, 1 (1993).
11. Bartholomew, C. H., *in* "Catalyst Deactivation 1994" (B. Delmon and G. F. Froment, Eds.), p. 1. Elsevier Science, Amsterdam, 1994.
12. Bartholomew, C. H., *in* "Catalyst Deactivation 1997" (C. H. Bartholomew and G. A. Fuentes, Eds.), p. 585. Elsevier Science, Amsterdam, 1997.
13. Fuentes, G. A., and Ruiz-Trevino, F. A., *in* "Catalyst Deactivation 1991" (C. H. Bartholomew and J. B. Butt, Eds.), p. 637. Elsevier Science, Amsterdam, 1991.
14. Campbell, W. G., Lynch, D. T., and Wanke, S. E., *AIChE J.* **34**, 1528 (1988).
15. Lo, A., and Skodje, R. T., *J. Chem. Phys.* **111**, 2726 (1999).
16. Lo, A., and Skodje, R. T., *J. Chem. Phys.* **112**, 1966 (2000).
17. Tikare, V., and Cawley, J. D., *Acta Mater.* **46**, 1343 (1998).
18. Tikare, V., and Holm, E. A., *J. Am. Ceram. Soc.* **81**, 480 (1998).
19. Wagner, D. D., *J. Phys. Chem. Ref. Data*, **11**, suppl. 2 (1982).
20. Stuckless, J. T., Starr, D. E., Bald, D. J., and Campbell, C. T., *J. Chem. Phys.* **107**, 5547 (1997).
21. Jennison, D. R., and Bogicevic, A., *Surf. Sci.* **464**, 108 (2000).
22. Kelber, J. A., Niu, C. Y., Shepherd, K., Jennison, D. R., and Bogicevic, A., *Surf. Sci.* **446**, 76 (2000).
23. Anderson, J. R., "Structure of Metallic Catalysts." Academic Press, New York, 1975.
24. Metropolis, N., Rosenbluth, A. W., Rosenbluth, M. N., Teller, A. N., and Teller, E., *J. Chem. Phys.* **21**, 1087 (1953).
25. Limoge, Y., and Bocquet, J. L., *Acta Metall.* **36**, 1717 (1988).
26. Tikare, V., Ph.D. dissertation. Case Western Reserve University, Cleveland, OH, 1994.
27. Bartholomew, C. H., *in* "Catalysis Volume 10" (J. J. Spivey and S. K. Agarwal, Eds.), p. 41. Royal Soc. Chem., Cambridge, U.K., 1993.
28. Xu, Q., Kharas, K. C. C., and Datye, A. K., *Stud. Surf. Sci. Catal.* **139**, 157 (2001).
29. Hassold, G. N., and Holm, E. A., *Comp. Phys.* **7**, 97 (1993).
30. Wright, S. A., Plimpton, S. J., Swiler, T. P., Fye, R. M., Young, M. F., and Holm, E. A., "Potts-Model Grain Growth Simulations: Parallel Algorithms and Applications," Sandia Report SAND97-1925. Sandia National Laboratories, Albuquerque, NM, 1997. (Available from National Technical Information Service, U.S. Department of Commerce, 5285 Port Royal Rd, Springfield, VA 22161.)
31. Sanders, L. M., and Datye, A. K., unpublished results.